THE JOURNAL OF BIOLOGICAL CHEMISTRY VOL. 283, NO. 34, pp. 23113–23120, August 22, 2008

Crystal Structure of the Human Fe65-PTB1 Domain*[S]

Received for publication, February 1, 2008, and in revised form, May 21, 2008 Published, JBC Papers in Press, June 11, 2008, DOI 10.1074/jbc.M800861200

Jens Radzimanowski[‡], Stéphanie Ravaud[‡], Sabine Schlesinger[‡], Joachim Koch[§], Konrad Beyreuther[¶], Irmgard Sinning[‡], and Klemens Wild[‡1]

From the [‡]Heidelberg University Biochemistry Center, INF328, D-69120 Heidelberg, [§]Institute of Biochemistry, Biocenter, Johann Wolfgang Goethe-University, Max-von-Laue-Strasse 9, D-69438 Frankfurt am Main, and [¶]Center of Molecular Biology, University of Heidelberg, INF282, D-69120 Heidelberg, Germany

The neuronal adaptor protein Fe65 is involved in brain development, Alzheimer disease amyloid precursor protein (APP) signaling, and proteolytic processing of APP. It contains three protein-protein interaction domains, one WW domain, and a unique tandem array of phosphotyrosine-binding (PTB) domains. The N-terminal PTB domain (Fe65-PTB1) was shown to interact with a variety of proteins, including the low density lipoprotein receptor-related protein (LRP-1), the ApoEr2 receptor, and the histone acetyltransferase Tip60. We have determined the crystal structures of human Fe65-PTB1 in its apo- and in a phosphate-bound form at 2.2 and 2.7 Å resolution, respectively. The overall fold shows a PTB-typical pleckstrin homology domain superfold. Although Fe65-PTB1 has been classified on an evolutionary basis as a Dab-like PTB domain, it contains attributes of other PTB domain subfamilies. The phosphotyrosine-binding pocket resembles IRS-like PTB domains, and the bound phosphate occupies the binding site of the phosphotyrosine (Tyr(P)) within the canonical NP*X*pY recognition motif. In addition Fe65-PTB1 contains a loop insertion between helix α2 and strand β2 (α2/β2 loop) similar to members of the Shc-like PTB domain subfamily. The structural comparison with the Dab1-PTB domain reveals a putative phospholipid-binding site opposite the peptide binding pocket. We suggest Fe65-PTB1 to interact with its target proteins involved in translocation and signaling of APP in a phosphorylation-dependent manner.

Fe65 is an adaptor protein predominantly expressed in the brain, where it plays a critical role in neuronal development and APP[2] signaling (1, 2). Fe65 exhibits three protein-protein interaction domains with different binding specificities as follows: one N-terminal WW domain and two contiguous C-terminal phosphotyrosine-binding domains (PTB1 and PTB2). The Fe65-WW domain recognizes polyproline sequences in several proteins, including c-Abl tyrosine kinase (3) and the mammalian homolog of the *Drosophila* actin cytoskeleton regulatory protein enabled (Mena) (4). The Fe65-PTB1 domain has been shown to interact with the low density lipoprotein receptor-related protein (LRP-1) (5), the ApoEr2 receptor (6), the histone acetyltransferase Tip60 (7), and the transcription factor CP2/LSF/LBP1 (8), whereas Fe65-PTB2 interacts with the APP intracellular domain (9). The Fe65-mediated multiprotein complexes are involved in diverse processes, including learning and memory (10), regulation of neuronal growth cone motility (11, 12), APP translocation and processing (13–15), and transcriptional regulation of gene expression (7, 16–20). Fe65-PTB1 is essential for many of these functions. In particular, the described interactions with Tip60 and CP2/LSF/LBP1 are important for the regulation of gene expression (7, 8), whereas the interaction with the C-terminal domain of LRP-1 has been shown to play a critical role for APP localization and processing (5) and therefore for Alzheimer disease pathogenesis.

PTB domains are protein-protein interaction modules recognizing short peptide regions, including the canonical NP*X*pY consensus sequence (sometimes reduced to N*XX*pY; *X* indicates relaxed residue selectivity) (21). PTB domains differ in their specificities for phosphorylated or unphosphorylated tyrosines, and most of the analyzed PTB domains bind their substrates in a Tyr(P)-independent manner. Based on evolutionary and structural comparisons, the PTB domains have been classified in three different subfamilies as follows: the Tyr(P)-dependent IRS-like and Shc-like PTB domains, and the Tyr(P)-independent Dab-like PTB domains (22). All PTB domains include the pleckstrin homology (PH) domain superfold consisting of seven antiparallel β-strands forming two orthogonal β-sheets (β-sandwich) capped by a C-terminal α-helix. The peptide binding pocket is mainly formed by the β5-strand and the C-terminal α-helix. In addition, many PTB domains contain a basic phospholipid binding "crown" located on the opposite site of the peptide binding pocket (22). Shc- and Dab-like PTB domains contain two additional α-helices, one located N-terminally and one inserted between the strands β1 and β2. Shc-like PTB domains contain also a large loop insertion between helix α2 and strand β2 (α2/β2 loop).

Here we report the first structure of a Fe65-PTB domain, Fe65-PTB1, in its apo- and in a phosphate-bound form at 2.2 and 2.7 Å, respectively. Although Fe65-PTB1 has been clas-

* This work was supported by Deutsche Forschungsgemeinschaft Grants WI2649/1-1 and WI2649/1-2 (to K. W.). The costs of publication of this article were defrayed in part by the payment of page charges. This article must therefore be hereby marked "*advertisement*" in accordance with 18 U.S.C. Section 1734 solely to indicate this fact.

The atomic coordinates and structure factors (codes 3D8D, 3D8E, and 3D8F) have been deposited in the Protein Data Bank, Research Collaboratory for Structural Bioinformatics, Rutgers University, New Brunswick, NJ (http://www.rcsb.org/).

[S] The on-line version of this article (available at http://www.jbc.org) contains supplemental Tables S1 and S2 and additional references.

[1] To whom correspondence should be addressed. Tel.: 49-6221-544785; Fax: 49-6221-544790; E-mail: klemens.wild@bzh.uni-heidelberg.de.

[2] The abbreviations used are: APP, amyloid precursor protein; PTB, phosphotyrosine-binding; PH, pleckstrin homology; ITC, isothermal titration calorimetry; r.m.s.d., root mean square deviation; IP_3, inositol 1,4,5-triphosphate; PDB, Protein Data Bank.

sified as a Dab-like PTB-domain, its structure reveals characteristics of different PTB domain subfamilies. The data presented here set the stage for an atomic understanding of a molecular crossroad of APP metabolism and Alzheimer disease pathogenesis.

EXPERIMENTAL PROCEDURES

Structure Determination—Expression, purification, and crystallization of Fe65-PTB1 (residues Gly-366 to Glu-505) as well as X-ray data collection were performed as described (23). The structure of Fe65-PTB1 was determined by single wavelength anomalous diffraction collected on a mercury derivative crystal ($P2_12_12_1$ space group) (23). Phasing was performed with the program suite PHENIX (Python-based Hierarchical Environment for Integrated Xtallography) (24, 25). After density modification, phases were of sufficient quality for automatic model building. The PHENIX-AUTOBUILD routine was able to build 230 residues (and the C-α traces of 22 additional amino acids) of the two molecules (A and B) in the asymmetric unit. The model was completed using iterative cycles of model building in COOT (26) and refinement with REFMAC5 (27, 28). Refinement statistics are given in Table 1. The refined model was used as a search model to solve the native structure (H3 space group) (23) by molecular replacement using program PHASER (29). Model building and refinement were performed as for the derivative structure (Table 1). Fe65-PTB1 complexed with phosphate was obtained by soaking native crystals (H3 space group) for 10 min in the crystallization buffer containing 50 mM Na_2HPO_4. Data collection statistics are presented in supplemental Table S1. The phosphate-bound structure was subsequently solved by difference Fourier technique using the native structure and refined as the other models (Table 1). The quality of all models was validated with programs PROCHECK (30) and WHAT-IF (31). The secondary structure was analyzed with program DSSP (32). Surface potentials were calculated with program GRASP (33), and figures were generated with programs MOLSCRIPT (34), Raster3D (35), and PyMOL.

Isothermal Titration Calorimetry—All isothermal titration calorimetry (ITC) experiments were carried out in a buffer containing 10 mM HEPES, pH 7.5, and 150 mM NaCl. Fe65-PTB1 and the respective peptides were extensively dialyzed against the same buffer. Solutions were degassed immediately before measuring, and all binding experiments were performed using a VP-ITC microcalorimeter (MicroCal, Northampton, MA) equilibrated at the desired temperature (15 or 25 °C). For all measurements the cell was filled with 20 μM peptide or inositol 1,4,5-triphosphate (IP_3), and 200 μM of purified Fe65-PTB1 was used as the titrant in the syringe. A typical titration consisted of injections of 12-μl aliquots of the titrant into the solution in the cell under constant stirring at 300 rpm at time intervals of 5 min to ensure that the titration peak returned to the base line. For data analysis the Origin 7.0 software was used.

Immobilized Peptide Libraries—Immobilized peptide libraries representing residues Met-229 to Trp-513 of the histone acetyltransferase domain of human Tip60 (10- and 15-mer peptides both tyrosine-phosphorylated and unphosphorylated with either one or three residue shifts) were synthesized as described previously (36, 37). After 2 h blocking with 4% (w/v) skim milk (Sigma) in the incubation buffer (20 mM K_2HPO_4, pH 6.8, 100 mM KCl, 50 mM NaCl, 2 mM $MgCl_2$, 1 mM $CaCl_2$, and 0.05% (v/v) Tween 20), the membranes were incubated with 0.25 μM purified Fe65-PTB1 in the incubation buffer for 1 h at 20 °C. Bound Fe65-PTB1 was detected with an anti-His antibody (Qiagen) and visualized using an enhanced chemiluminescence (ECL) anti-mouse IgG secondary antibody (GE Healthcare). Incubations with the antibodies were performed in the incubation buffer supplemented with 0.5% (w/v) skim milk. All incubation steps were followed by three consecutive wash steps of 10 min in the incubation buffer.

TABLE 1
Refinement statistics

Refinement statistics	Derivative, $P2_12_12_1$ apo	Native, H3 apo	Native, H3 phosphate-bound
Resolution (Å)	42-2.2	25-2.8	50-2.7
R_{cryst} (%)[a]	20.2	24.0	24.2
R_{free} (%)[b]	25.2	30.4	31.3
Average *B*-factor (Å^2)	35.5	59.8	59.9
Phosphate ions			86.9
No. if non-hydrogen atoms			
Protein	2180	3835	3969
Phosphate ions			2
Mercury	6		
Ethylene glycol	4		
Water	130		22
r.m.s.d. bonds (Å)	0.015	0.016	0.014
r.m.s.d. angles (°)	1.45	1.78	1.64
Ramachandran plot			
Most favored (%)	92.6	89.0	85.7
Additionally allowed (%)	7.4	11.0	13.8

[a] $R_{cryst} = \Sigma\|F_{obs}| - |F_{calc}\|/\Sigma|F_{obs}|$.
[b] $R_{free} = R_{cryst}$ for 5–10% of all data.

Phospholipid Binding Assays—A membrane lipid strip (PIP-strip, Echelon) pre-spotted with a solvent blank control and 15 different biologically abundant lipids found in cell membranes was blocked at 20 °C for 1 h in PBST buffer (2.7 mM KCl, 4.3 mM Na_2HPO_4, 1.8 mM KH_2PO_4, 137 mM NaCl, and 0.1% (v/v) Tween 20, pH 7.2) supplemented with 3% (w/v) skim milk (Sigma) and afterward incubated at 20 °C for 1 h in the same buffer containing 1–100 μg/ml Fe65-PTB1. Bound Fe65-PTB1 was detected with an anti-His antibody (Qiagen) and visualized using an ECL anti-mouse IgG secondary antibody (GE Healthcare).

RESULTS AND DISCUSSION

Structure Determination of Fe65-PTB1—The N-terminal PTB domain of human Fe65 (Fe65-PTB1, residues Gly-366 to Glu-505) crystallized in the two space groups H3 (native crystals; four molecules per asymmetric unit) and $P2_12_12_1$ (derivative crystals; two molecules per asymmetric unit). The orthorhombic space group was metal-induced as the result of co-crystallization experiments with methyl mercury chloride as described previously (23). The crystal structure was determined at 2.2 Å resolution by single wavelength anomalous diffraction using a mercury derivative crystal. The native structure (H3 space group) was determined by molecular replacement at 2.8 Å resolution. Refinement statistics are given in Table 1.

In the $P2_12_12_1$ space group, the two molecules of the asymmetric unit are well ordered except two residues (Gly-460 and Arg-461) in a loop region. The root mean square deviation (r.m.s.d.) between the $P2_12_12_1$ and the H3 structures has an average of 0.74 Å for all C-α atoms. The main differences occur

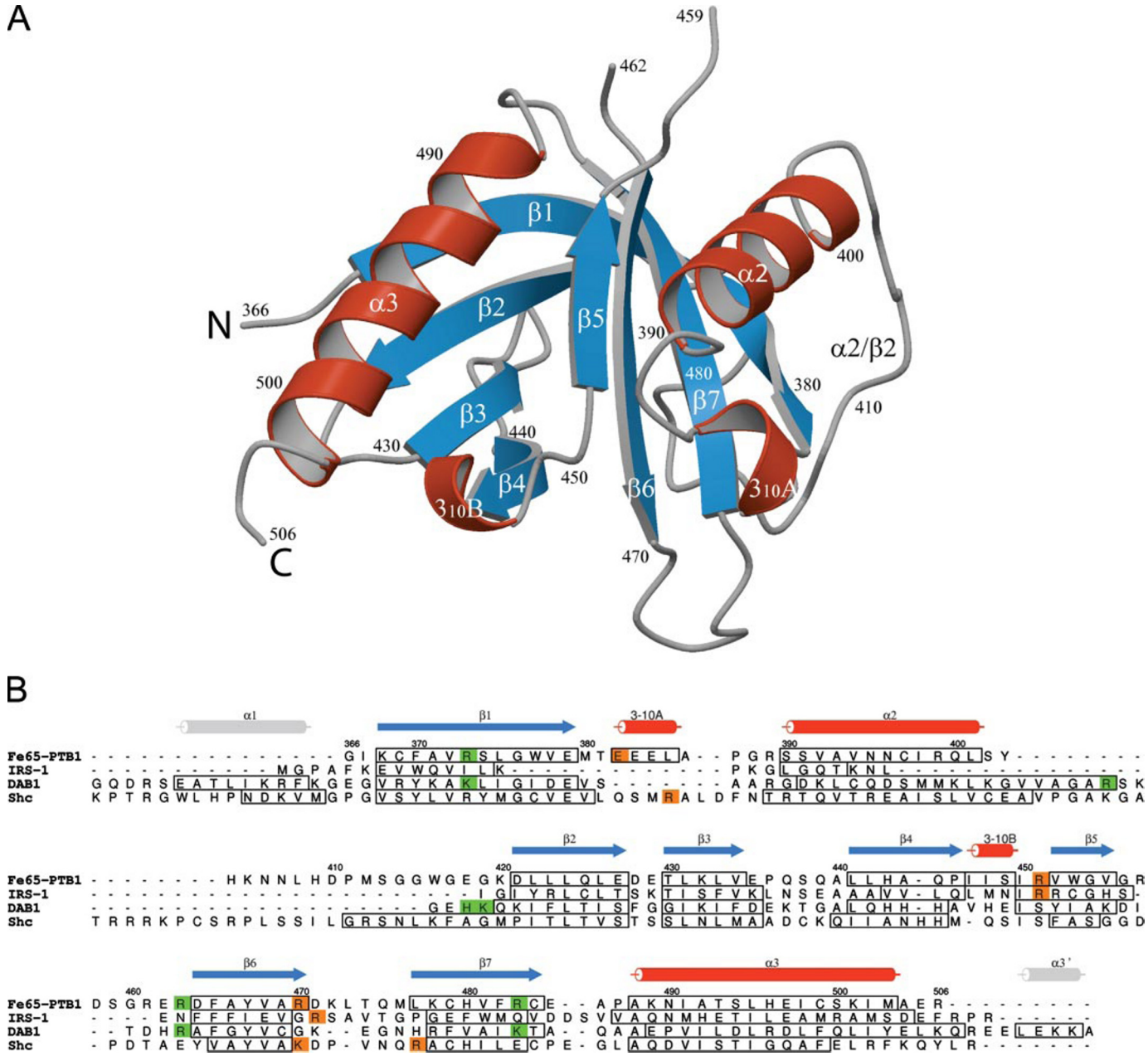

FIGURE 1. **Structure of Fe65-PTB1.** *A*, overall structure model of Fe65-PTB1 colored according to secondary structure. N and C termini, secondary structure elements, and every 10th residue are labeled. *B*, structure-based sequence alignment of Fe65-PTB1 with representative members from each PTB domain subfamily. Numbering and secondary structure assignment above the sequences corresponds to Fe65-PTB1. Within each sequence, the respective secondary structures are *boxed*. Additional secondary structure elements of other PTB domains are shown in *gray*. Residues involved in phosphotyrosine binding are highlighted in *orange*. Dab1-PTB residues interacting with the phospholipid headgroup IP_3 and their Fe65-PTB1 equivalents are shaded in *green*.

in a loop region comprising residues Gln-400 to Lys-420 (see below). In the H3 space group this region is mostly not visible in the electron density.

Overall Structure of Fe65-PTB1—The structure of the Fe65-PTB1 domain reveals the folding pattern of the pleckstrin homology (PH) domain superfold (Fig. 1*A*). The core of this fold consists of seven antiparallel β-strands ($\beta1$–$\beta7$) arranged in two orthogonal β-sheets. This β-sandwich is capped by a C-terminal α-helix ($\alpha3$). Additional structural features of the PH domain superfold are also present in Fe65-PTB1. These include the peptide binding pocket formed by strand $\beta5$, helix $\alpha3$, and the $\beta1/\alpha2$ loop, and a putative phospholipid-binding site next to the $\alpha2/\beta2$ loop (see below).

On an evolutionary basis, Fe65-PTB1 has been grouped into the Dab-like PTB domain subfamily (22). Consistent with this classification, an analysis of the Fe65-PTB1 structure using the Dali server (38) identified Dab-like PTB domains as the closest structural relatives (for details see supplemental Table S2). However, sequence identities are relatively low (below 25%), and the r.m.s.d. values of about 2.0 Å indicate significant structural differences between Fe65-PTB1 and Dab-like PTB domains.

The $\alpha1$-helix located at the N terminus of Shc- and Dab-like PTB domains (Fig. 1*B* and Fig. 2) is not present in the Fe65-PTB1 structure and is not predicted on the sequence level. Like most PTB domains, Fe65-PTB1 includes one additional helix

(α2) located between the β1- and β2-strands (Fig. 1 and Fig. 2). Fe65-PTB1 reveals a unique β1/α2 loop (residues Met-380 to Arg-389) with an inserted 3_{10} helix (3_{10}A, residues Glu-382 to Leu-385) as part of the phosphotyrosine-binding pocket. The α2/β2 loop is extended (residues Gln-400 to Lys-420), which is a characteristic feature of the Shc subfamily of PTB domains where this loop has accordingly been termed as Shc loop (22). However, this extended loop is also present in the Dab-like X11-PTB domain (39). In the $P2_12_12_1$ space group this loop is involved in crystal contacts and is part of the model. However, in the structures derived from the H3 space group, the α2/β2 loop is not present indicating a high conformational flexibility.

Phosphate Binding to Fe65-PTB1 Suggests Phosphotyrosine-dependent Peptide Interactions—The overall mode of peptide binding is conserved in all PTB domain structures determined so far (Fig. 2). PTB-binding peptides fold in *trans* as an antiparallel β-strand on top of strand β5 and are aligned parallel to the C-terminal helix α3. The consensus sequence fingerprint of PTB-binding peptides consists of the NP*X*pY motif. NP*X*pY motifs are typical internalization signals for membrane-associated receptor proteins (40–42). This sequence has a high propensity of forming a β-turn structure, which in all PTB domains is specifically read out by an "anchoring" binding pocket harboring most of the peptide binding energy especially in the Tyr(P)-dependent interactions (43).

The three PTB domain subfamilies differ significantly in (phospho)-tyrosine recognition (Fig. 2). In Dab-like PTB domains, the anchoring pocket has only a minor role in peptide recognition, and tyrosine phosphorylation often decreases the binding affinity (39, 44, 45). On the contrary, IRS-like and Shc-like PTB domains require phosphorylated tyrosines for high affinity binding (46–48). The Shc-like PTB domains use three basic residues (two arginines and one lysine) to accommodate the Tyr(P) residue (46). The IRS-1 structure reveals two other arginine residues at different locations, which create a basic pocket for the negatively charged phosphate moiety (48). Fe65-PTB1 contains two equivalent arginine residues (Arg-451 and Arg-470) at the same position as IRS-1. Arg-451 is involved in a tight salt bridge with Glu-382, which is located in the unique 3_{10} helix (3_{10}A) of the β1/α2 loop (Fig. 3*A*).

To test for a phosphorylation dependence of peptide binding to Fe65-PTB1, we soaked native Fe65-PTB1 crystals with phosphate and determined the structure at 2.7 Å resolution (see supplemental Table S1 for data collection statistics and Table 1 for refinement statistics). The binding of phosphate into the pocket could be confirmed by prominent difference densities in the unbiased difference density maps (Fig. 2). The occupancy for the phosphate is 75%, and together with the phosphate concentration of 50 mM used in the soaking experiments a K_d value in the range of 20 mM can be estimated. Phosphate binding in the Fe65-PTB1 structure is exclusively performed by the two arginine residues Arg-451 and Arg-470 (Fig. 3*A*). Although the terminal nitrogen N-ϵ2 of Arg-451 forms a single hydrogen bond to phosphate oxygen, Arg-470 orients the phosphate

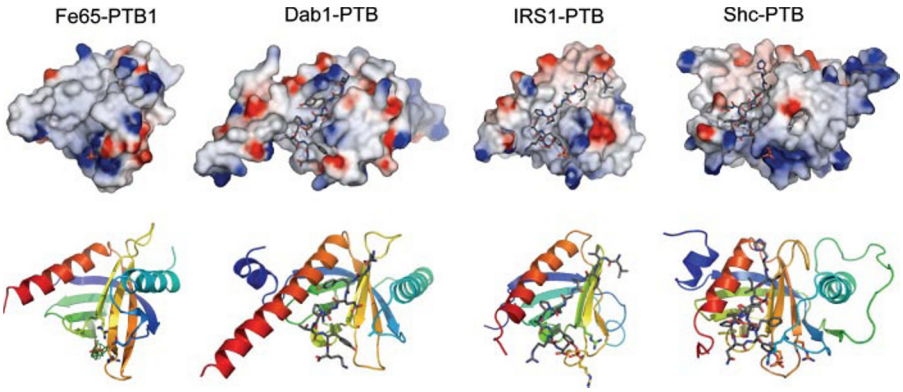

FIGURE 2. **Comparison of Fe65-PTB1 with representative structures of the three PTB subfamilies bound to peptides.** *Top row,* electrostatic surface potentials. Positive and negative patches on the protein surfaces are given in *blue* and *red,* respectively. Bound ligands are given as *stick models*. All proteins have the same orientation. *Bottom row,* structure models of the respective PTB domains in a color ramping from *blue* (N terminus) to *red* (C terminus). The unbiased $F_o - F_c$ difference electron density for the phosphate in the Fe65-PTB1 structure is given at a 2σ level.

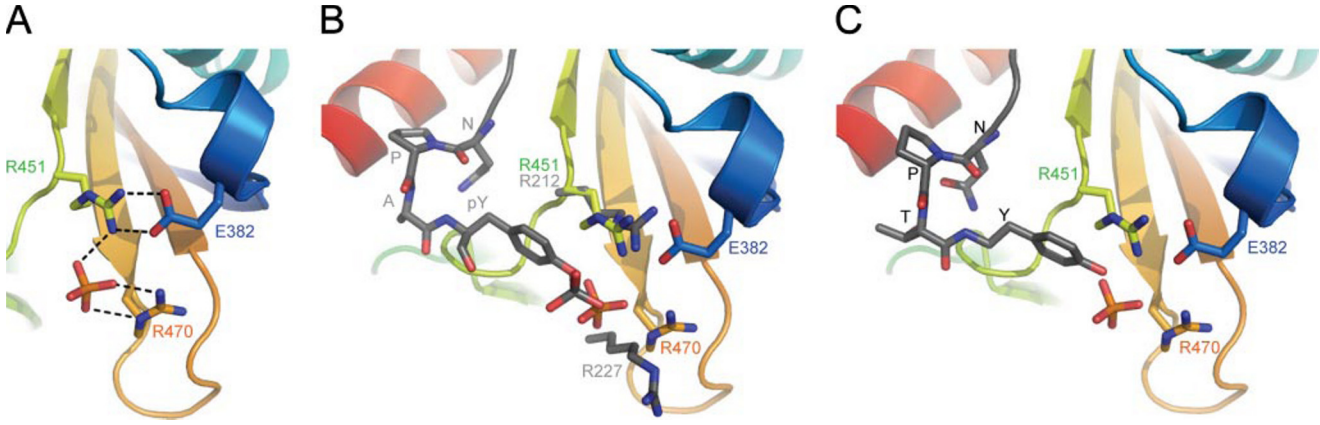

FIGURE 3. **Phosphate binding to Fe65-PTB1 suggests phosphotyrosine-dependent peptide interactions.** *A*, close-up view of the Fe65-PTB1 Tyr(P) binding pocket. The hydrogen-bonding network of the phosphate group is indicated by *dashed lines*. *B*, superposition of phosphate-bound Fe65-PTB1 with the IRS-1 PTB domain (PDB code 1irs). The bound NPApY motif of the bound peptide to IRS-1 is shown together with the two respective IRS-1 arginine residues of the binding pocket (*gray*). *C*, phosphate-bound Fe65-PTB1 superposed to the Dab1/APP nonphosphorylated peptide, including the NPTY motif (PDB code 1oqn).

by two hydrogen bonds with its guanidinium group. Although the charge of Arg-451 is partially neutralized by the interaction with Glu-382, it will contribute to phosphate binding due to the nondirected character of Coulomb interactions. In addition to phosphate binding, the conserved Arg-451 is perfectly located to stabilize a putative phosphotyrosine binding by a π-cation stacking interaction of the aromatic ring with the planar guanidinium group.

When phosphate-bound Fe65-PTB1 is superposed on the IRS-1 PTB domain complexed with a phosphorylated interleukin-4 receptor peptide (48), the phosphate groups are found to bind in the same position and orientation (Fig. 3*B*). Therefore, we assume the bound phosphate group in Fe65-PTB1 to mimic the phosphate moiety of a phosphorylated peptide indicating a phosphorylation dependence of peptide recognition. The binding mode of the two arginines to the phosphate moiety of Tyr(P) is, however, slightly different. In IRS-1 the arginine residue (Arg-212) equivalent to Arg-451 in Fe65-PTB1 is not stabilized by a salt bridge, and the whole binding pocket is more open compared with Fe65-PTB1. Interestingly, the corresponding arginine to Arg-470 (Arg-227) is not involved in direct hydrogen bonding with the phosphate in the IRS-1 structure. The tighter binding of the phosphate moiety suggests at least an equal preference of Fe65-PTB1 for phosphorylated substrates.

Similarly, when the Dab1 structure in complex with an unphosphorylated APP peptide (49) is overlaid on Fe65-PTB1, the hydroxyl of the bound APP tyrosine matches with the phosphate oxygen that is hydrogen-bonded to Arg-451 (Fig. 3*C*). In Dab1, however, the binding pocket lacks the two arginine residues, and the binding of a nonphosphorylated tyrosine is favored (49, 50). The $\beta1/\alpha2$ loop in Dab1 also contributes to the binding pocket but via an alanine residue. The Fe65-PTB1 residue Glu-382 located on helix 3_{10}A is not conserved in Dab1.

In summary, peptide binding to Fe65-PTB1 is likely to be Tyr(P)-dependent as deduced from the conservation of the binding pocket and the binding mode of the bound phosphate moiety. The conservation of the binding pocket reveals a relationship in peptide binding to IRS-like PTB domains.

Interaction with Putative Binding Partners—The histone acetyltransferase Tip60 was identified as a Fe65-PTB1 binding partner in a study performed by Cao and Sudhof (7) using a gene reporter assay and pulldown experiments with an N-terminal truncated Tip60β construct. This construct does not include the typical NP*X*Y motif but two N*XX*Y motifs within the histone acetyltransferase domain. The mutation of the ^{257}NKSY motif into ^{257}NASA was shown to abolish the interaction between Fe65-PTB1 and Tip60 suggesting this motif to be a putative binding site. However, structural modeling of Fe65-PTB1 onto the recently solved Tip60HAT structure (PDB code 2ou2), assuming the conserved PTB/NP*X*Y binding mode, is not possible because of the different structural environment of the ^{257}NKSY motif. This motif does not form the characteristic β-turn structure but is completely embedded into an α-helix with the tyrosine being buried in the interior of the protein. Therefore, to investigate further the interaction and to discriminate between the two N*XX*Y-binding motifs, we performed ITC experiments at different temperatures using synthesized 11-mer peptides, including either the ^{242}NEIY or the ^{257}NKSY sequence (phosphorylated and unphosphorylated; Table 2). However, none of the tested peptides revealed a significant binding to Fe65-PTB1 indicating a K_D >300 μM (data not shown). To test if binding of Fe65-PTB1 occurs at another site, we sampled the complete Tip60HAT sequence in an immobilized peptide library approach using a library of overlapping 10- or 15-mer peptides (with phosphorylated and unphosphorylated tyrosines). Although we found some positive hits for surface patches (including both N*XX*Y motifs) predominantly located opposite of the acetyl-CoA binding cleft, both N*XX*Y motifs showed up in the phosphorylated and nonphosphorylated state, which neither allowed for a discrimination of the two sites nor for a clarification of the phosphorylation dependence (data not shown).

TABLE 2
Peptides used in ITC measurements

Protein fragments	Sequence
Tip60β(237–247)	RHPPGNEIYRK
	RHPPGNEIpYRK
Tip60β(251–261)	EIDGRKNKSYS
	EIDGRKNKSpYS
LRP-1(4465–4576)	NVEIGNPTYKMY
	NVEIGNPTpYKMY
LRP-1(4498–4510)	PTNFTNPVYATL
	PTNFTNPVpYATL
ApoEr2(858–869)	SMNFDNPVYRKT
	SMNFDNPVpYRKT

In addition to Tip60, we also tested the proposed interactions of FE65-PTB1 with the intracellular domains of the lipoprotein receptors LRP-1 and ApoEr2 (5, 6). Again, we used synthesized peptides, including the NP*X*Y motifs (^{4470}NPTY, ^{4503}NPVY for LRP-1, and ^{863}NPVY for ApoEr2) in both the phosphorylated and unphosphorylated forms (Table 2) in ITC experiments. To our surprise and like for Tip60, none of the peptides showed binding to Fe65-PTB1 (data not shown).

In summary, the proposed interactions with Fe65-PTB1 could not be validated. As Fe65-PTB1 is stable in solution and experimental parameters like concentrations and temperature in the ITC experiments were carefully checked and modified, we assume either a low affinity binding or the requirement for a specific cellular environment or more complete protein fragments of the interaction partners.

Membrane Attachment—In addition to direct protein-protein interactions, many PTB domains were shown to be involved in membrane attachment (for review see Ref. 22). Direct membrane recruitment of PTB domains allows for a reduction of dimensionality, local concentration within specific membrane compartments like lipid rafts, and pre-orients the domain for favorable interactions with their membrane-bound peptide substrates. Similar to the pleckstrin homology (PH) domains, binding occurs to headgroups of phosphoinositides. Phosphoinositides show a unique subcellular distribution dependent on the degree and position of headgroup phosphorylation (51). They play a fundamental role in the spatial and temporal control of many signaling processes at membrane-cytosol interfaces. Of special interest is phosphatidylinositol 4,5-biphosphate, which has an important function in endocytosis events at the plasma membrane (49, 52).

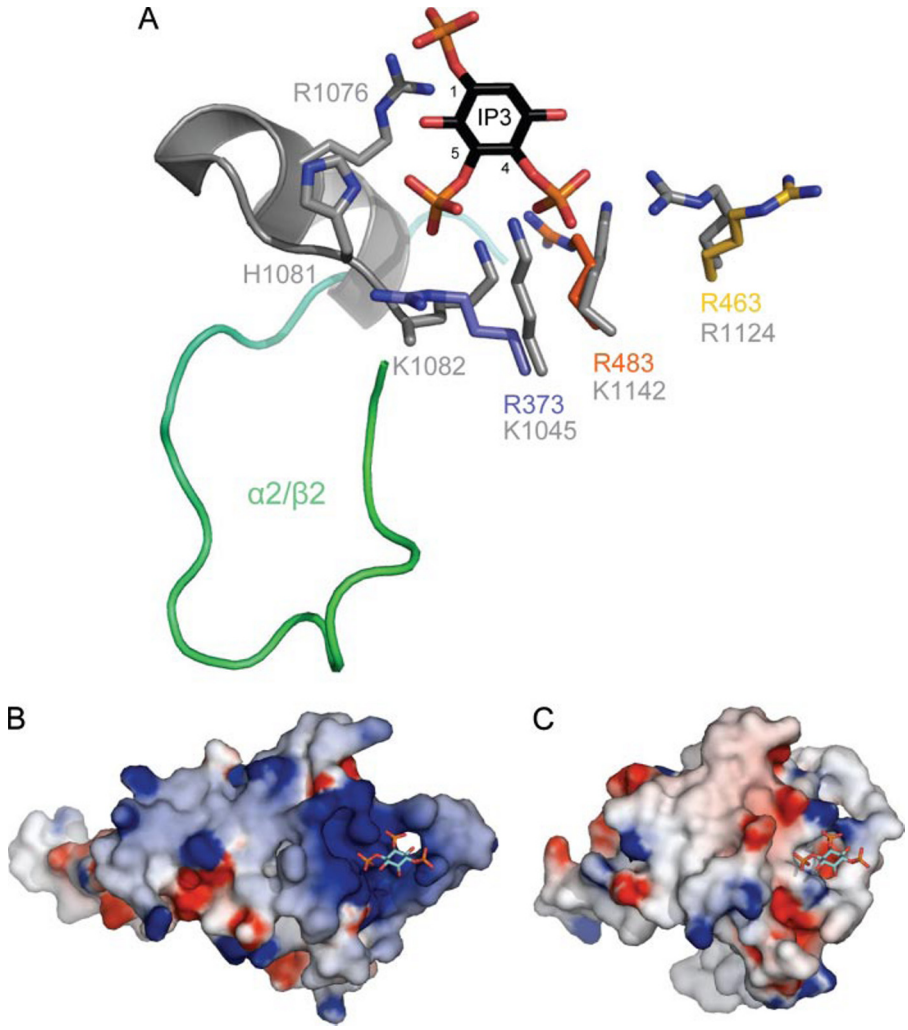

FIGURE 4. **The putative phospholipid-binding site.** *A*, Fe65-PTB1 (color ramps as in Figs. 2 and 3) superposed with the Dab1-PTB-APP-IP_3 complex (PDB code 1oqn) shown in *gray* and *black*. Residues involved in IP_3 binding and the equivalent three arginines of Fe65-PTB1 are given. Although helix α2 in Dab1 is elongated by two turns, Fe65-PTB1 contains a long and flexible α2/β2 loop. *B*, electrostatic surface potential of the Dab1-PTB domain showing the highly positively charged phospholipid binding crown responsible for IP_3 binding (*stick model*). Color scheme is as in Fig. 2. *C*, Fe65-PTB1 oriented in the same way with superposed IP_3 taken from the Dab1-PTB structure.

The structural basis for phosphatidylinositol 4,5-biphosphate binding to PTB domains has been revealed by crystal structures of the ternary complexes of Dab1-PTB with the phospholipid headgroup IP_3 and either an ApoEr2 (50) or APP peptide (49). In the Dab1 protein the PTB domain is essential for membrane recruitment and reveals high affinity binding for IP_3 ($K_D \sim 0.7\ \mu M$) (53) and a highly positively charged surface patch opposite to the peptide binding pocket and oriented toward the membrane (52). The pocket is located at the C-terminal end of helix α2 and involves the adjacent α2/β2 loop as well as a set of basic residues from or next to the rigid β-sheet core (β1, β6, and β7) (Fig. 4*A*). It has been assigned by three-dimensional electrostatic analysis to form a basic crown (22) (Fig. 4*B*). Strikingly, the superposition of the ternary complexes with the Fe65-PTB1 structure reveals a conservation of one-half of the basic pocket, including three basic residues originating from the β-sheet core (Arg-373, Arg-463, and Lys-483 in Fe65-PTB1) (Fig. 4*A*). In Dab1, these residues are responsible for recognition of the phosphates at positions four and five of IP_3. Despite the conservation of positively charged residues, however, a pronounced phospholipid-binding crown is not present within Fe65-PTB1 (Fig. 4*B*). As in Dab1-PTB, helix α2 is elongated by two turns and the α2/β2 loop is much shorter, and the second half of the binding pocket recognizing the phosphates at positions one and five cannot be correlated on the sequence level (Fig. 1*B*). Although Fe65-PTB1 contains several basic residues in this region (Lys-405, His-409, and Lys-420), their spatial orientation in the Fe65-PTB1 structure is different as compared with the Dab1-PTB complexes. However, the α2/β2 loop of Fe65-PTB1 is flexible, as deduced by comparison of the structures from the two different space groups, and therefore it might adopt a conformation favorable for phospholipid binding.

We investigated the putative binding of Fe65-PTB1 to phosphoinositides by immobilized lipid-protein binding assays (PIP-strips), ITC, and co-crystallization experiments. In the PIP-strip assays, we could not detect binding to any of the tested lipids or phospholipids, including different mono-, di-, and tri-phosphorylated phosphoinositides. Similarly, ITC and co-crystallization experiments with IP_3 under various conditions did not reveal binding to Fe65-PTB1 (data not shown).

Taken together, although Fe65-PTB1 reveals distinct features for phospholipid binding, we could not detect a direct interaction. However, the structural and functional homology between Fe65-PTB1 and the Dab1-PTB domain as well as previous studies on other PTB domains (for review see Ref. 22) make an interaction under physiological conditions very likely.

Conclusions—The Fe65-PTB1 domain shares the pleckstrin homology domain superfold and is structurally closely related to the Dab-like PTB domain subfamily. The comparison of Fe65-PTB1 with Dab1 reveals distinct features of a phospholipid-binding site, although the interaction could not be validated experimentally. In Dab1, the interaction is strong and essential for membrane recruitment. However, Fe65 is mainly recruited to the membrane by its interaction with the APP intracellular domain. In the close proximity to the membrane even a weak phospholipid binding of Fe65-PTB1 might therefore be sufficient to attach and to orient the domain at the membrane surface.

The structure of Fe65-PTB1 reveals as well unique and Dab-unlike characteristics. Most strikingly is the Tyr(P) binding pocket that resembles IRS-like PTB domains. Phosphate binding to Fe65-PTB1 indicates a Tyr(P) dependence of substrate interactions. Fe65-PTB1 would therefore be the first Tyr(P)-dependent and Dab-like PTB domain. A phosphorylation dependence of Fe65-PTB1 interactions has a significant impact on our current understanding of APP translocation and signaling events. Noteworthy, the intracellular domain of APP binds to Fe65-PTB2 in a Tyr(P)-independent manner (9). Fe65-PTB1 is the cross-point that links APP to the lipoprotein receptors LRP-1 and ApoEr2 and to the transcription regulators Tip60 and CP2/LSF/LBP1, although we were not able to validate interactions in our experiments and further studies are needed to define the exact molecular mechanisms. However, it seems that yet to be identified kinases are important for Fe65-mediated multiprotein complex formation.

Finally, the various Fe65-mediated interactions are well known to play an essential role for APP processing and amyloid-β generation (54). The accumulation of the amyloid-β peptide is a central event in the pathogenesis of Alzheimer disease, and the peptide is the main constituent of the senile plaques. Elucidating the molecular details of the pathways leading to amyloid-β formation is therefore both promising and necessary for a successful treatment of the devastating disease.

Acknowledgments—We are grateful to I. Groemping from the Max-Planck-Institute for Medical Research (Heidelberg, Germany) for help with ITC measurements. We acknowledge access to beamlines ID14-eh2, ID23-1, and ID29 at the European Synchrotron Radiation Facility (ESRF) in Grenoble, France, and the excellent support by the beamline scientists.

REFERENCES

1. King, G. D., and Scott Turner, R. (2004) *Exp. Neurol.* **185,** 208–219
2. Guenette, S., Chang, Y., Hiesberger, T., Richardson, J. A., Eckman, C. B., Eckman, E. A., Hammer, R. E., and Herz, J. (2006) *EMBO J.* **25,** 420–431
3. Zambrano, N., Bruni, P., Minopoli, G., Mosca, R., Molino, D., Russo, C., Schettini, G., Sudol, M., and Russo, T. (2001) *J. Biol. Chem.* **276,** 19787–19792
4. Ermekova, K. S., Zambrano, N., Linn, H., Minopoli, G., Gertler, F., Russo, T., and Sudol, M. (1997) *J. Biol. Chem.* **272,** 32869–32877
5. Trommsdorff, M., Borg, J. P., Margolis, B., and Herz, J. (1998) *J. Biol. Chem.* **273,** 33556–33560
6. Hoe, H. S., Magill, L. A., Guenette, S., Fu, Z., Vicini, S., and Rebeck, G. W. (2006) *J. Biol. Chem.* **281,** 24521–24530
7. Cao, X., and Sudhof, T. C. (2001) *Science* **293,** 115–120
8. Zambrano, N., Minopoli, G., de Candia, P., and Russo, T. (1998) *J. Biol. Chem.* **273,** 20128–20133
9. Borg, J. P., Ooi, J., Levy, E., and Margolis, B. (1996) *Mol. Cell. Biol.* **16,** 6229–6241
10. Wang, B., Hu, Q., Hearn, M. G., Shimizu, K., Ware, C. B., Liggitt, D. H., Jin, L. W., Cool, B. H., Storm, D. R., and Martin, G. M. (2004) *J. Neurosci. Res.* **75,** 12–24
11. Sabo, S. L., Ikin, A. F., Buxbaum, J. D., and Greengard, P. (2001) *J. Cell Biol.* **153,** 1403–1414
12. Sabo, S. L., Ikin, A. F., Buxbaum, J. D., and Greengard, P. (2003) *J. Neurosci.* **23,** 5407–5415
13. Sabo, S. L., Lanier, L. M., Ikin, A. F., Khorkova, O., Sahasrabudhe, S., Greengard, P., and Buxbaum, J. D. (1999) *J. Biol. Chem.* **274,** 7952–7957
14. Santiard-Baron, D., Langui, D., Delehedde, M., Delatour, B., Schombert, B., Touchet, N., Tremp, G., Paul, M. F., Blanchard, V., Sergeant, N., Delacourte, A., Duyckaerts, C., Pradier, L., and Mercken, L. (2005) *J. Neurochem.* **93,** 330–338
15. Pietrzik, C. U., Yoon, I. S., Jaeger, S., Busse, T., Weggen, S., and Koo, E. H. (2004) *J. Neurosci.* **24,** 4259–4265
16. Kimberly, W. T., Zheng, J. B., Guenette, S. Y., and Selkoe, D. J. (2001) *J. Biol. Chem.* **276,** 40288–40292
17. Cao, X., and Sudhof, T. C. (2004) *J. Biol. Chem.* **279,** 24601–24611
18. Telese, F., Bruni, P., Donizetti, A., Gianni, D., D'Ambrosio, C., Scaloni, A., Zambrano, N., Rosenfeld, M. G., and Russo, T. (2005) *EMBO Rep.* **6,** 77–82
19. Hass, M. R., and Yankner, B. A. (2005) *J. Biol. Chem.* **280,** 36895–36904
20. Sumioka, A., Nagaishi, S., Yoshida, T., Lin, A., Miura, M., and Suzuki, T. (2005) *J. Biol. Chem.* **280,** 42364–42374
21. Smith, M. J., Hardy, W. R., Murphy, J. M., Jones, N., and Pawson, T. (2006) *Mol. Cell. Biol.* **26,** 8461–8474
22. Uhlik, M. T., Temple, B., Bencharit, S., Kimple, A. J., Siderovski, D. P., and Johnson, G. L. (2005) *J. Mol. Biol.* **345,** 1–20
23. Radzimanowski, J., Ravaud, S., Beyreuther, K., Sinning, I., and Wild, K. (2008) *Acta Crystallogr. Sect. F* **64,** 382–385
24. Adams, P. D., Grosse-Kunstleve, R. W., Hung, L. W., Ioerger, T. R., McCoy, A. J., Moriarty, N. W., Read, R. J., Sacchettini, J. C., Sauter, N. K., and Terwilliger, T. C. (2002) *Acta Crystallogr. Sect. D Biol. Crystallogr.* **58,** 1948–1954
25. Adams, P. D., Gopal, K., Grosse-Kunstleve, R. W., Hung, L. W., Ioerger, T. R., McCoy, A. J., Moriarty, N. W., Pai, R. K., Read, R. J., Romo, T. D., Sacchettini, J. C., Sauter, N. K., Storoni, L. C., and Terwilliger, T. C. (2004) *J. Synchrotron Radiat.* **11,** 53–55
26. Emsley, P., and Cowtan, K. (2004) *Acta Crystallogr. Sect. D Biol. Crystallogr.* **60,** 2126–2132
27. Collaborative Computational Project, No. 4 (1994) *Acta Crystallogr. Sect. D Biol. Crystallogr.* **50,** 760–763
28. Murshudov, G. N., Vagin, A. A., and Dodson, E. J. (1997) *Acta Crystallogr. Sect. D Biol. Crystallogr.* **53,** 240–255
29. McCoy, A. J. (2007) *Acta Crystallogr. Sect. D Biol. Crystallogr.* **63,** 32–41
30. Laskowski, R. A., Rullmannn, J. A., MacArthur, M. W., Kaptein, R., and Thornton, J. M. (1996) *J. Biomol. NMR* **8,** 477–486
31. Vriend, G. (1990) *J. Mol. Graphics* **8,** 52–56
32. Kabsch, W., and Sander, C. (1983) *Biopolymers* **22,** 2577–2637
33. Nicholls, A., Sharp, K. A., and Honig, B. (1991) *Proteins* **11,** 281–296
34. Kraulis, P. J. (1991) *J. Appl. Crystallogr.* **24,** 946–950
35. Merritt, E. A., and Murphy, M. E. (1994) *Acta Crystallogr. Sect. D Biol. Crystallogr.* **50,** 869–873
36. Groves, M. R., Mant, A., Kuhn, A., Koch, J., Dubel, S., Robinson, C., and Sinning, I. (2001) *J. Biol. Chem.* **276,** 27778–27786
37. Koch, J., and Mahler, M. (eds) (2002) *Peptide Arrays on Membrane Supports*, pp. 83–96, Springer Verlag, Heidelberg, Germany
38. Holm, L., and Sander, C. (1996) *Methods Enzymol.* **266,** 653–662
39. Zhang, Z., Lee, C. H., Mandiyan, V., Borg, J. P., Margolis, B., Schlessinger, J., and Kuriyan, J. (1997) *EMBO J.* **16,** 6141–6150
40. Lai, A., Sisodia, S. S., and Trowbridge, I. S. (1995) *J. Biol. Chem.* **270,** 3565–3573
41. Koo, E. H., and Squazzo, S. L. (1994) *J. Biol. Chem.* **269,** 17386–17389
42. Chen, W. J., Goldstein, J. L., and Brown, M. S. (1990) *J. Biol. Chem.* **265,** 3116–3123
43. Farooq, A., Plotnikova, O., Zeng, L., and Zhou, M. M. (1999) *J. Biol. Chem.* **274,** 6114–6121
44. Howell, B. W., Lanier, L. M., Frank, R., Gertler, F. B., and Cooper, J. A. (1999) *Mol. Cell. Biol.* **19,** 5179–5188
45. Dho, S. E., Jacob, S., Wolting, C. D., French, M. B., Rohrschneider, L. R., and McGlade, C. J. (1998) *J. Biol. Chem.* **273,** 9179–9187
46. Zhou, M. M., Ravichandran, K. S., Olejniczak, E. F., Petros, A. M., Meadows, R. P., Sattler, M., Harlan, J. E., Wade, W. S., Burakoff, S. J., and Fesik, S. W. (1995) *Nature* **378,** 584–592
47. Eck, M. J., Dhe-Paganon, S., Trub, T., Nolte, R. T., and Shoelson, S. E. (1996) *Cell* **85,** 695–705
48. Zhou, M. M., Huang, B., Olejniczak, E. T., Meadows, R. P., Shuker, S. B., Miyazaki, M., Trub, T., Shoelson, S. E., and Fesik, S. W. (1996) *Nat. Struct.*

Biol. **3,** 388–393
49. Yun, M., Keshvara, L., Park, C. G., Zhang, Y. M., Dickerson, J. B., Zheng, J., Rock, C. O., Curran, T., and Park, H. W. (2003) *J. Biol. Chem.* **278,** 36572–36581
50. Stolt, P. C., Jeon, H., Song, H. K., Herz, J., Eck, M. J., and Blacklow, S. C. (2003) *Structure* (*Lond.*) **11,** 569–579
51. Di Paolo, G., and De Camilli, P. (2006) *Nature* **443,** 651–657
52. Wolf, G., Trub, T., Ottinger, E., Groninga, L., Lynch, A., White, M. F., Miyazaki, M., Lee, J., and Shoelson, S. E. (1995) *J. Biol. Chem.* **270,** 27407–27410
53. Stolt, P. C., Vardar, D., and Blacklow, S. C. (2004) *Biochemistry* **43,** 10979–10987
54. McLoughlin, D. M., and Miller, C. C. (2008) *J. Neurosci. Res.* **86,** 744–754